First principles assessment of the phase stability and transition mechanisms of designated crystal structures of pristine and Janus transition metal dichalcogenides

First Principles Assessment on Phase Stability and Transition Mechanisms of Designated Crystal Structures of Pristine and Janus Transition Metal Dichalcogenides

Öznur Demirkol[a], Cem Sevik[b,c] and İlker Demiroğlu[d*]

[a] *Department of Physics, Eskisehir Technical University, Eskişehir, TR 26470, Turkey.*
[b] *Department of Mechanical Engineering, Eskişehir Technical University, Eskisehir, TR 26555, Turkey.*
[c] *Department of Physics, University of Antwerp, Groenenborgerlaan 171, 2020 Antwerp, Belgium*
[d] *Department of Advanced Technologies, Eskisehir Technical University, Eskisehir, TR 26555, Turkey.*
[*] E-mail: ilkerdemiroglu@eskisehir.edu.tr

Abstract

Two-dimensional Transition Metal Dichalcogenides (TMDs) possessing their extraordinary physical properties at reduced dimensionality have attracted interest due to their promise in electronic and optical device applications. However, the TMD monolayers can show a broad range of different properties depending on their crystal phase, for example H phases are usually semiconductor while the T phases are metallic. Thus, controlling phase transitions become critical for device applications. In this study, the energetically low-lying crystal structures of pristine and Janus TMDs are investigated by using ab-initio Nudged Elastic Band and molecular dynamics simulations to provide a general explanation for their phase stability and transition properties. Across all materials investigated, the T phase is found to be the least stable and the H phase is the most stable except for WTe_2, while T' and T'' phases change places according to the TMD material. The transition energy barriers are found to be large enough to hint that even the higher energy phases are unlikely to go under a phase transition to a more stable phase if they can be achieved except for the least stable T phase which has zero barrier towards T' phase. Indeed, in molecular dynamics simulations the thermodynamically least stable T phase transformed into T' phase spontaneously while in general no other phase transition was observed up to 2100 K for the other three phases. Thus, the examined T', T'' and H phases were shown to be mostly stable and does not readily transform into another phase. Furthermore, so-called mixed phase calculations considered in our study explain the experimentally observed lateral hybrid structures and point out that the coexistence of different phases are strongly stable against phase transitions. Indeed, stable complex structures such as metal-semiconductor-metal architectures, which have immense potential to be used in future device applications, are also possible based on our investigation.

Keywords: Molybdenum, Tungsten, disulfide, ditelluride, diselenide, molecular dynamics, density functional theory, multiphase, coexistence

1. Introduction

Two-dimensional (2D) materials have attracted interest of many material scientists around the globe due to their extraordinary properties in contrast to their three-dimensional (3D) counterparts. Primarily in 2004, graphene flake was isolated from highly oriented pyrolytic graphite and its peculiar electronic and other physical properties were investigated [1]. It is found that its physical properties were interestingly different from its 3D counterpart: graphite due to reduced dimensions. [2] To date, It has been demonstrated that 2D materials show incredible properties such as tunable band gap [3], high carrier mobility [4], increased chemical stability [5], tunable optical properties [6], superconductivity [7] and high mechanical strength [8]. Beginning from the isolation of graphene, many 2D materials with unique properties are investigated. Transition metal dichalcogenides (TMDs), which have interesting electrical and optical properties, [9] have become one of the most intensely studied structures among 2D materials. TMDs have forbidden band gaps at bulk, however their electronic properties change from indirect to direct in monolayers, which allows their usage in technological applications such as transistors and photodetectors [10,11]. As there is inherently a larger variety of accessible crystalline phases at 2D scale, different phases of 2D-TMDs provides challenging properties for fundamental research and applications [12]. 2D monolayer TMDs consist of three sublayers of atoms: The same two chalcogen (X) atom sublayers and one transition metal (M) atom sublayer placed between them. The bulk TMDs show different phases depending on the relative location between sublayers and the atoms setting in each sublayer. The four phases of MX_2 are known as H, T, T' and T''. Electronic and physical properties can be altered within 2D TMDs by controlling phase transition between semiconducting H phase and semimetallic or metallic T phases such as T, T' and T'' [13,14].

Most of the TMD monolayers have in-plane inversion symmetry. Nonetheless, few TMD monolayers are semiconductor with direct band gaps, due to their in-plane asymmetry. This asymmetry results in outstanding optical properties and optoelectronic applications [15]. Along with this in-plane inversion asymmetry; spin manipulation, which is allowed with additional degree of freedom, can be done by applying an external electric field or creating an asymmetric out-of-plane structural configuration, thus breaking out-of-plane mirror symmetry [16,17]. For

Example, if the upper sulfur atomic layer of the MoS_2 monolayer is replaced by the selenium atomic layer, it distorts the out-of-plane mirror symmetry, thereby forming a Janus type monolayer [18]. 2D Janus monolayers can be shown in the form of MXY where the X chalcogen layer is replaced by another type (Y) chalcogen layer. Due to their lack of mirror symmetry, Janus TMDs (MXY) have a reduced C_{3v} symmetry while MX_2 type monolayers have D_{3v} symmetry [18]. Furthermore, the charge distribution of Janus TMDs are not uniform between top and bottom atomic layers, due to differences in electronegativities and atomic radii of different elements which they are consists of [19]. Indeed, Janus TMDs have been successfully fabricated through CVD methods [16,20,21] and their several unique properties such as strong Rashba spin splitting, a second-harmonic generation response, large piezoelectric effect, and good catalytic performance have been reported in literature. [22]

Both Janus and pristine TMD structures may have different phases; such as H, T, T', T" and phase transitions between those phases are possible under proper conditions, which can be utilized for improved technological properties. [23,24] Thus, thermodynamical and kinetical stabilities of these phases and the transition energy barriers among them would be very helpful for fundamental applications of these different phases of monolayer materials in nanoscale devices.

On the other hand, lateral heterostructures with different phases of TMDCs has also been experimentally achieved. [25,26] This is utmost important due to the future device applications because these lateral hybrid materials with different electronic structures may lead to complex material architectures within a single material. Therefore, the systematic determination of structure stability and energetic properties of these hybrid materials are critical.

In this paper, we investigated crystalline phases of MX_2 and MXY type 2D-TMDs (M=Mo, W; X, Y=S, Se, Te) and possible phase transitions between them by using ab-initio techniques. Thermal stabilities of different phases are analysed by ab-initio molecular dynamics (AIMD) simulations. The energy barriers for phase transitions are calculated with climbing image nudged elastic band (CI-NEB) method by using the Vienna Ab initio Simulation Package (VASP) within the density functional theory (DFT).

2. Computational Details

All the calculations including structural optimizations, CI-NEB and AIMD simulations were performed with the Vienna Ab-initio-Simulation-Package (VASP) [27,28] code by using Density Functional Theory (DFT). Perdew-Burke Ernzerhof (PBE) flavour of the generalized gradient approximation (GGA) is used for exchange-correlation functional within DFT [29,30]. The monolayer TMD structures are constructed as 2x2x1 supercells consisting of 24 atoms. In order to calculate monolayer structures within the VASP code, a vacuum distance of at least 15 Å in the vertical direction is ensured to eliminate spurious interactions between the periodic structures in z-direction. A gamma point centered Monkhorst-Pack grid [31] of 5x3x1 k-points is used for Brillouin zone sampling. The cut off energy for plane-wave basis expansion is set to 500 eV within projector augmented wave (PAW) method [32,33]. All DFT calculations were performed until the forces on the ions are less than 0.01 eV / Å. The total energy convergence limit is set to 10^{-6} eV for electronic part of the minimization.

The transition energy barriers of pristine and Janus TMDs were calculated by climbing image nudged elastic band (CI-NEB) method via Transition State Tools for VASP (VTST) [34,35]. As CI-NEB method searches the lowest energy pathway between two given related structures, it is adopted to compute the energy barriers for the transitions between the H, T, T', and T'' phases. By carefully analyzing all the phase structures, we matched all individual atoms to minimize individual movement of atoms during the phase transition before the CI-NEB calculations. A 5-image pathway is calculated between these constructed terminal structures within the CI-NEB approach.

AIMD simulations were performed with a timestep of 1 fs within NPT ensemble (constant particle, pressure, and temperature) [36]. Initial AIMD simulations are first performed to heat the structures to room temperature for all considered phases, which is considered as equilibration part. Then room temperature simulations are conducted for further 5000 steps. Finally heating simulations with a 600 K/fs increase rate up to 900K, 1500K and 2100K are performed respectively for most of the systems until the structure becomes into a 'melted' state if not showing a distinct phase transition.

3. Results and Discussion

Pristine monolayers (MX_2) are first modelled by two layers of the same chalcogen atom (X= S, Se, Te), and then the Janus monolayers (MXY) are modelled from the replacement of one X layer by another type chalcogen atom (Y= S, Se, Te). We have considered four different possible crystal phases, which are distinguished by the coordinates of chalcogen atoms in respect to M atom. In H phase, the X atoms are AA-stacked because of transition metal atoms occupy the trigonal prismatic voids. In T phase, M atoms occupy octahedral voids between AB-stacked chalcogen atoms. T′ phase can be seen as a reconstruction of T phase where the connectivity is the same while there is an alternating order of chalcogen atoms getting closer and away to the plane and hence the metal atoms getting closer or further to their neighbours. Finally, T′′ phase is known as 'mixed phase', which can be seen as a series of H and T′ phases merged together. The Figure 1 shows crystal structures of these four different phases for pristine TMDs.

To find the optimum structural parameters for each system, the energy changes for each lattice parameter are independently optimized. Then the equation of state curves are obtained by the variance of the area corresponding to these optimized lattice parameters. The optimized lattice parameters of pristine and Janus monolayers are listed in Table 1. The calculated lattice parameters are in very good agreement (less than %2 differences in general) with the existing literature for all considered pristine TMD phases [37–40] and the Janus phases of H and T′ [41–43].

In general, the calculated lattice parameters both for MX_2 and MXY monolayers increase with the increasing atomic radius of chalcogen atoms. It is found that the optimized b lattice parameters of pristine and Janus TMDs are very close to half of the b′ lattice parameters for T′′ phases as the conventional unit cell for T′′ phase is double of other phases in the y direction. Although the a parameter do not vary much between the phases, the b parameter of T′ phase is the largest among all phases and the b′/2 is the second highest for T′′ phase. This is due to the reconstructions of the chalcogen atoms in these phases on xy plane causing an increase in the metal-metal distances in y direction.

The total energy per formula unit as a function of area (equation of state) for optimized atomic structures of pristine and Janus TMDs for H, T, T′, T′′ phases were given in Figure 2. The

chemical/energetical stabilities of H, T, T′ and T′′ phases of pristine and Janus TMDs were investigated by comparing equation of states (lower energy means better stability). Across all materials investigated, the T phase is found to be the least chemically/energetically stable phase while the H phase is the most chemically stable phase except for WTe_2. However, note that the energy differences for the other Te containing TMDs such as $MoTe_2$ and WSeTe, the energy difference between H and T′ is only below 0.02 eV. For WTe_2, T′ phase is found to be the most stable and the energy difference with H phase is 0.03 eV. Energetically, the approximate stabilities of T′ and T′′ phases are found close to each other for most of the materials investigated (in general below 0.04 eV except for WTe_2). T′ phase is slightly more stable than T′′ phase in $MoTe_2$, WTe_2, WSe_2, MoSeTe, WSTe and WSeTe and vice versa for the other TMDs considered. In other words, in all the S containing TMDs except for WSTe T′′ is more favourable than T′. When we compare the pristine and the Janus TMD, the general tendency is that the energy differences between phases decreased for Janus TMDs by 0.03 eV than in pristine TMDs.

To investigate the possible phase transitions between these energetically proximate phases, CI-NEB calculations are conducted both for pristine and Janus TMDs. Different possible transition paths between different phases are all considered. Figure 3 displays the lowest transition energy profiles of different phase transitions calculated by CI-NEB, which shows the energies of initial, transition and final states, respectively. For H↔T, H↔T′, H↔T′′, T′′↔T′ transitions, a transition state occurs between two corresponding local minima phase. These transition state structures are given in Supplementary Information S17. However, there is no transition state between T↔T′ transitions, which hints a spontaneous transformation and thus T phase cannot be regarded as a true local minimum. This is also in line with the observed negative frequencies on the phonon dispersion curves of T phase $MoTe_2$[44], while there are no imaginary frequencies for any of the H-phase phonon examples of both pristine[45] and janus TMDs[19]. In literature, there exist also stable phonon spectrum examples of T′-MoS_2,[46] WS_2,[46] WTe_2,[47] MoSSe,[48] MoSTe,[48] and T′′- MoS_2[49]. Calculated phonon dispersion curves of all four phases of MoS_2, MoSSe, $MoSe_2$, WS_2, WSSe, and WSe_2 are also given in Supplementary Information S18-S21.

The calculated transition energy barrier values are all listed in Table 2. For all pristine and Janus cases, the energy barrier of the transition from the H phase to the T phase (H→T) is the

largest among all phase transitions, and the values range between 1.08 eV and 1.70 eV. In general, second highest transition energy barrier values are found for H→T′ ranging between 0.69 eV and 1.51 eV. These higher energy barriers separate the H and T group structures and means more difficult transitions between them. The energy barrier of the transition from the H phase to the T″ phase (H→T″) is smaller than H→T and H→T′ transition energy barriers and its value is ranging between 0.51 eV and 0.99 eV. As the T″ structures are somehow a mixture of T′ and H phases, in general its transition to both ends has a very similar energy barrier. As these transition energy barriers from T″ are at least 0.2 eV, all these three phases can be regarded as local minima for both pristine and Janus TMDs. That being said, phase transitions including T″ are primarily expected if any as their energy barriers are the lowest, despite still being higher than 200 meV (For a rough Arrhenius equation type comparison, k_bT is 25.7 meV at room Temperature). When we compare the transition energy barriers of Janus TMDs (MXY) to their parent pristine TMDs (MX_2 or MY_2), either the energy barriers are increased relative to the both chalcogen atoms or the value is somewhere in the middle of the values for MX_2 and MY_2. Therefore, the phase transitions for Janus TMDs are as difficult as in the case for pristine TMDs, which also confirms the stability of all the three phases holds for Janus TMDs. For Janus TMDs, the energy differences between different phases are also lower than for corresponding pristine ones, while the transition energy barriers are not smaller. This implies that reaching other phases could be more feasible for Janus TMDs while they are expected as stable as pristine TMD phases.

When we compare our results to the existing literature, there is slight difference for the H→T and T→H barriers of MoS_2 with Pandey et al [50] where our values differ by around 0.2 eV. This is because it is difficult to get the barriers between H and T phases since the transition goes over T′ phase as Huang et al [37] discussed this in their work as well and our barrier values are within 0.02 with theirs for $MoTe_2$ and WTe_2. For the H→T′ and T′→H transitions of $MoTe_2$, we find almost the same values with Krishnamoorthy et al. [51] (0.77 eV and 0.71 eV, respectively). Moreover, all of our barrier energy values compare well with a more comprehensive work of Patil et al. [38], which covers all the barriers between H, T′ and T″ phases for MoS_2, $MoSe_2$, WS_2, and WSe_2.

To ensure the phase stabilities and to check the coexistence of multiple phases, we constructed a mixed phase (HT′) unit cell, which contains H and T′ phases partially. There are two and four

distinct possible merging configurations for pristine and Janus TMDs, respectively for such a HT' mixing. Among them the lowest energy configuration is actually equivalent to the T″ phase if merging only one unit from both H and T′ phases in the lateral direction. The idea behind is somehow excite the T′ phase by converting one half of the cell into more energetically favorable H phase in advance, to check whether the transition energy barriers are lowered or not. Otherwise it may also hint the stable coexistence of multiple phases. Indeed, such coexistence models are suggested [52,53] and experimentally observed [25,26] to engineer properties such as electronic transport. The Figure 4 shows the transition energy profile through such a HT′ mixed phase for MoS_2 and MoSSe. A significant reduction in the transition energy barriers was observed between H and T′ phases through this mixed HT′ phase: 0.97 eV for MoS2 and 0.76 eV for MoSSe. However, these lowered transition energy barriers and the barriers from the mixed HT′ phase itself are still over 0.33 eV, which give even a possibility to the coexistence of different phases together. When we compare the relative energies of larger HT′ mixed phase structures for Janus MoSSe (see supplementary info Table 1), where there are two and three units merged from H and T′ phases, energetic stability increases with the increasing number of units.

To further investigate the stabilities and the possible phase transitions of the considered phases, AIMD simulations were performed both for pristine and Janus TMDs. Room temperature AIMD simulations suggest that all phases except the T phase (H, T′ and T′′) are thermally stable for all pristine and Janus TMDs (see Figure 5 and Supplementary Information S3-S14). However, for both Janus and pristine structures, it is observed that T phase transitions into T′ phase beginning even from 5 K. In Figure 5, the WTe_2 and WSeTe examples are given as these systems have relatively lower transition energy barriers than the other systems. Their total energy fluctuation curves at room temperature show that the energetical order holds also for AIMD simulations, where the T′ phase is more stable in WTe_2 and H phase is more stable for WSeTe. Figure 5 also shows the temperature and energy fluctuation curves of the 5K AIMD simulations for T phase MoS_2 and MoSSe structures as an example for the spontaneous T→T′ phase transition. The instant temperature rise, and the corresponding potential energy drop coincide with the structural phase transition. Other AIMD simulations confirm this instability for the T phase for all pristine and Janus TMDs considered with very similar pictures (see Supplementary information S1 and S2).

Heating AIMD simulations were also carried out to check whether phase transitions or structural deformations will occur at higher temperatures for H, T′ and T′′ phases. Figure 6 shows example results for T′′-$MoTe_2$ and T′′-MoSeTe phases as these systems had relatively higher transition probabilities due to their relatively lower transition energy barriers. Temperature and energy fluctuations can be seen in these corresponding graphs in Figure 6 and the energy is increasing relative to the temperature increase in the heating AIMD runs. Although the atoms start to move faster at higher temperatures which result in local structural distortions at any time frame, the phase structures do not change or distort as the average positions of the atoms do not deviate drastically. However, heating materials above 1500K in general resulted in structural deformations like a melted state (example structures can be seen in the last column of Figure 6) instead of a phase transition until 2100K. Yet we did not characterize the exact melting temperatures as it would require orders of magnitude larger computational resources and will be out of scope of this study. Nonetheless, until 1500K, we did not observe any phase transition or structural deformation for any of the H, T′ and T′′ phases (see Figure 6 and supplementary information S3-S14), which hints a high thermal stability for these materials for H, T′ and T′′ phases for all considered TMD materials.

As in the CI-NEB calculations, to check the coexistence of the multiple phases, we repeated the AIMD simulations on the HT′, HT′′, and T′T′′ mixed phases of MoSSe structures, which contains two lateral units from each corresponding phase. In general, the total energy values of mixed phases (see Figure 7a) lie somewhere between the total energies of the original phases (see Figure 7b). Energetically HT′′ mixed phase has the lowest energy for MoSSe followed by HT′ and then T′T′′ phases as expected due to the energetical order of their component phases. To check how the lateral unit size effect the energetics of the mixed phases, AIMD simulations are done also for three lateral unit containing HT′ phase from each corresponding phase for MoSSe. As can be seen from the energetic analysis from these AIMD simulations (see supplementary information S16), the energetic stability increases with the lateral size of the coexisting phases. All the mixed phase AIMD simulations gave similar pictures in terms of temperature and energy fluctuations with the original phases and they preserved their multiphase structures during whole simulation. Furthermore, still no phase transition could be observed for these so-called excited phases up to the melting temperatures (see Figure 7 and

supplementary information S15-16). Thus, it is concluded that all the considered H, T′ and T′′ phases are thermally stable and even they may coexist together as mixed phases.

Conclusion

In summary, the structural and thermal stabilities of H, T, T′ and T′′ phases and their lateral coexistence for pristine and Janus TMDs were investigated by DFT calculations along with the energetics of transitions between them. The optimal structural parameters were characterized for each phase and their energetics are compared to observe their relative stabilities. Among all considered phases, H phase is found to be the most stable phase while T phase is the least stable one, except for WTe_2 material. By CI-NEB calculations, it was observed that the transition energy barriers from H phase to T phase is higher than the other phase transitions. In general, all the transition barriers among H, T′ and T′′ phases are found to be larger than 0.35 eV (except for T′′→T′ transition in WTe_2 and $MoTe_2$ which are around 0.2 eV), which hint that these phases are unlikely to go under a phase transition to a more stable phase if they can be achieved. AIMD simulations are conducted to check the thermal stability calculations starting from 300 K. Then the temperature was gradually increased to 2100 K with 600 K/fs. Apart from thermal fluctuations of the constituent atoms, the crystal structures remain unchanged up to 1500K for H, T′ and T′′ phases. However, even at 5K AIMD simulations revealed a spontaneous phase transition for T phase into T′, which is consistent with the instability of T phase. Hybrid phase calculations reveal that not only pristine but also Janus hybrid structures are possible, and their energetic stability increases with the lateral size of the coexisting phases.

To sum up, our results show high stability for H, T′ and T′′ phases both for pristine and Janus TMDs and the possibility of their coexistence as hybrid phases. Effectively controlling structural phases of 2D TMDs is very critical and may enable various potential applications in electronic, optic and spintronic devices and therefore we believe that Janus type multiple phase TMDs would be a valid direction for further experimental progress on such device technologies.

Table 1. The optimized lattice structure parameters (in Å) of H, T, T′, T′′ phases for pristine and Janus TMDs. For T′′ phase b′/2 is given in table for practical comparison with equivalent b parameter of other phases.

	H		**T**		**T′**		**T′′**	
Pristine	a	b	a	b	a	b	a	b′/2
MoS_2	3.18	5.52	3.18	5.53	3.18	5.73	3.19	5.66
$MoSe_2$	3.32	5.75	3.28	5.69	3.28	5.97	3.30	5.89
$MoTe_2$	3.55	6.15	3.49	6.06	3.43	6.40	3.51	6.27
WS_2	3.18	5.51	3.20	5.56	3.19	5.72	3.22	5.65
WSe_2	3.32	5.74	3.28	5.68	3.30	5.95	3.30	5.88
WTe_2	3.55	6.15	3.51	6.08	3.49	6.31	3.52	6.27
Janus	a	b	a	b	a	b	a	b′/2
MoSSe	3.25	5.63	3.22	5.58	3.22	5.86	3.25	5.77
MoSTe	3.36	5.83	3.32	5.75	3.32	6.08	3.36	5.96
MoSeTe	3.43	5.95	3.38	5.85	3.38	6.17	3.41	6.07
WSSe	3.25	5.63	3.24	5.62	3.24	5.84	3.25	5.77
WSTe	3.36	5.83	3.32	5.76	3.34	6.05	3.36	5.95
WSeTe	3.43	5.94	3.38	5.86	3.40	6.14	3.42	6.07

Table 2. Energy barrier values (eV/TMD unit) of structural phase transformation for pristine and Janus TMDs

Structures	H→T	T→H	H→T′	T′→H	H→T′′	T′′→H	T′′→T′	T′→T′′
MoS_2	1.55	0.71	1.51	0.96	0.92	0.45	0.50	0.42
$MoSe_2$	1.35	0.65	1.12	0.79	0.76	0.41	0.37	0.38
$MoTe_2$	1.08	0.56	0.77	0.73	0.57	0.40	0.23	0.36
WS_2	1.69	0.79	1.50	0.97	0.99	0.49	0.54	0.50
WSe_2	1.47	0.69	1.15	0.88	0.78	0.44	0.38	0.45
WTe_2	1.18	0.61	0.69	0.78	0.51	0.38	0.20	0.41
MoSSe	1.59	0.85	1.45	1.02	0.90	0.53	0.53	0.46
MoSTe	1.51	1.03	1.29	1.04	0.71	0.50	0.55	0.51
MoSeTe	1.39	0.86	1.09	0.92	0.70	0.51	0.43	0.46
WSSe	1.70	0.89	1.42	1.02	0.92	0.55	0.54	0.52
WSTe	1.59	1.05	1.26	1.08	0.76	0.57	0.57	0.58
WSeTe	1.48	0.89	1.07	1.00	0.68	0.52	0.41	0.51

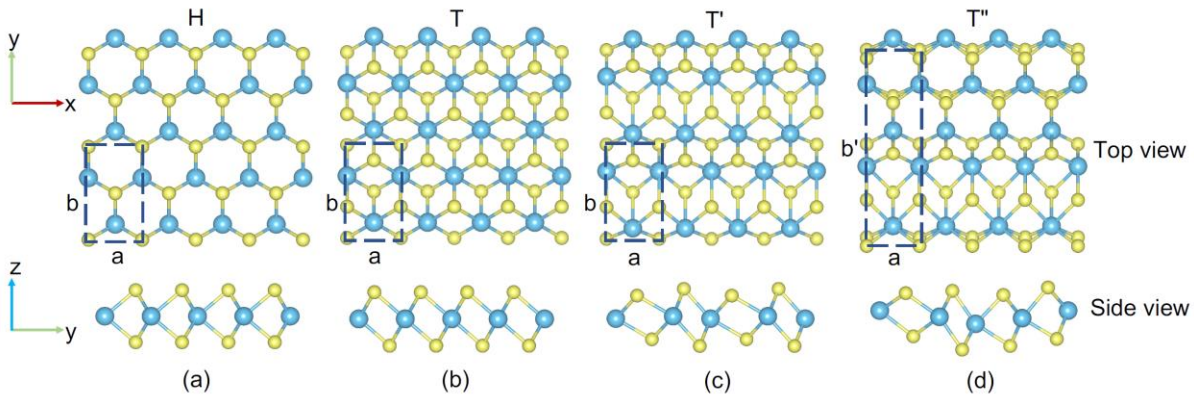

Figure 1. Top and side view of the atomic structures of monolayer pristine TMDs for (a) H, (b) T, (c) T′, (d) T′′ phases. Blue spheres represent the transition metal atom, whereas yellow spheres represent chalcogen atoms.

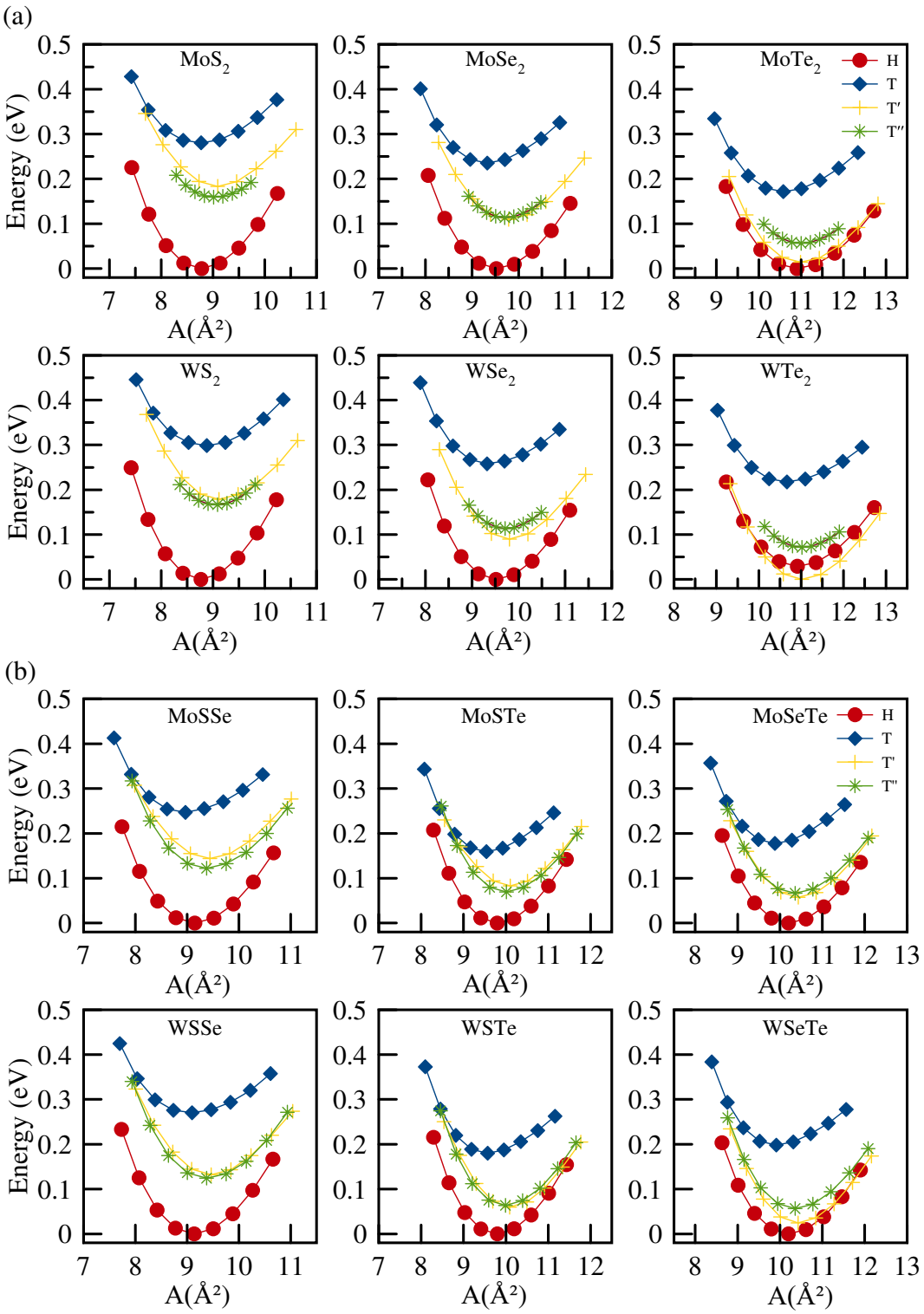

Figure 2. Equation of states of different phases of (a) pristine and (b) Janus TMDs including group VIB.

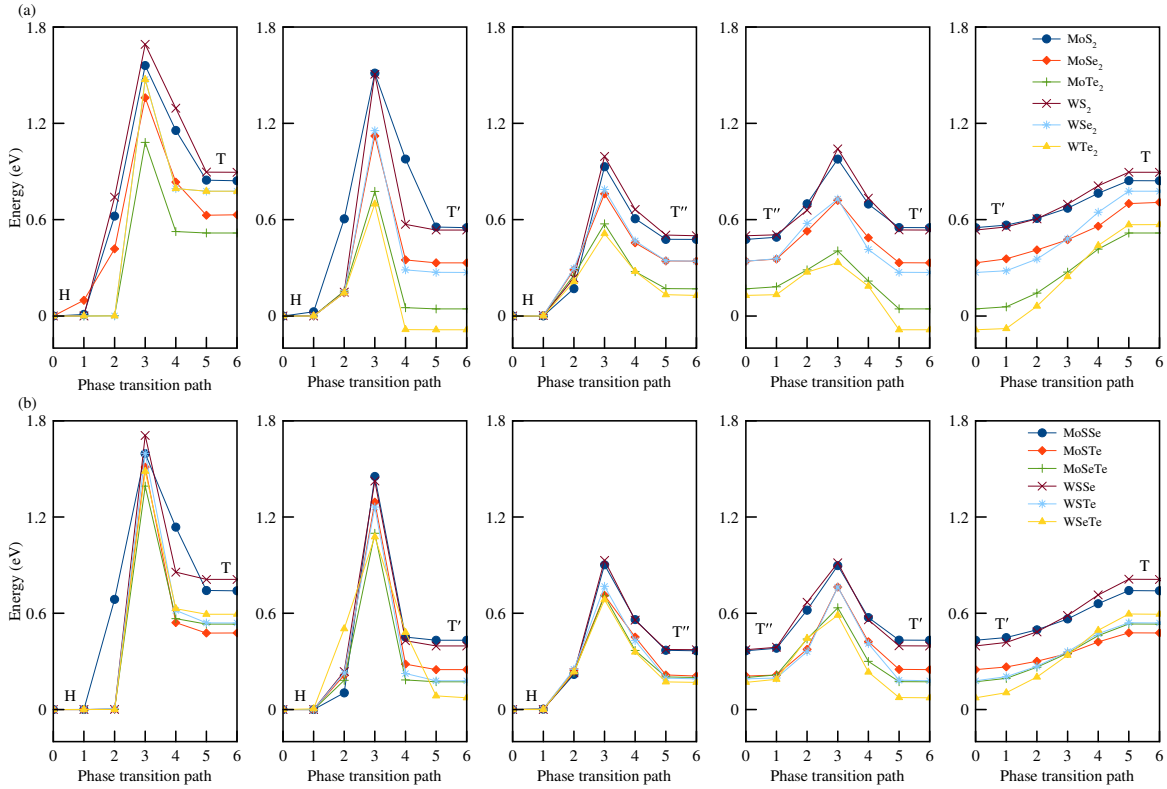

Figure 3. Change of (a) the pristine TMDs and (b) the Janus TMDs energy per chemical formula unit as a function of phase transition coordinate for (a) H↔T, (b) H↔T′, (c) H↔T′′, (d) T′′↔T′, (e) T′↔T phases.

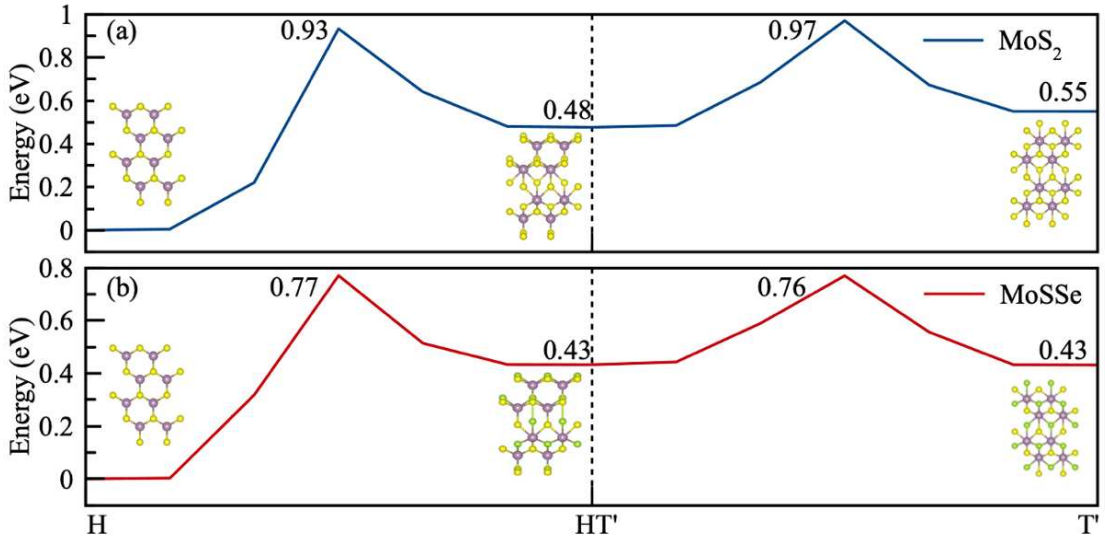

Figure 4. The relative energy difference and transition energy barrier between the H phase, H-T′ multiple phase and the T′ phase of (a) MoS2, (b) MoSSe.

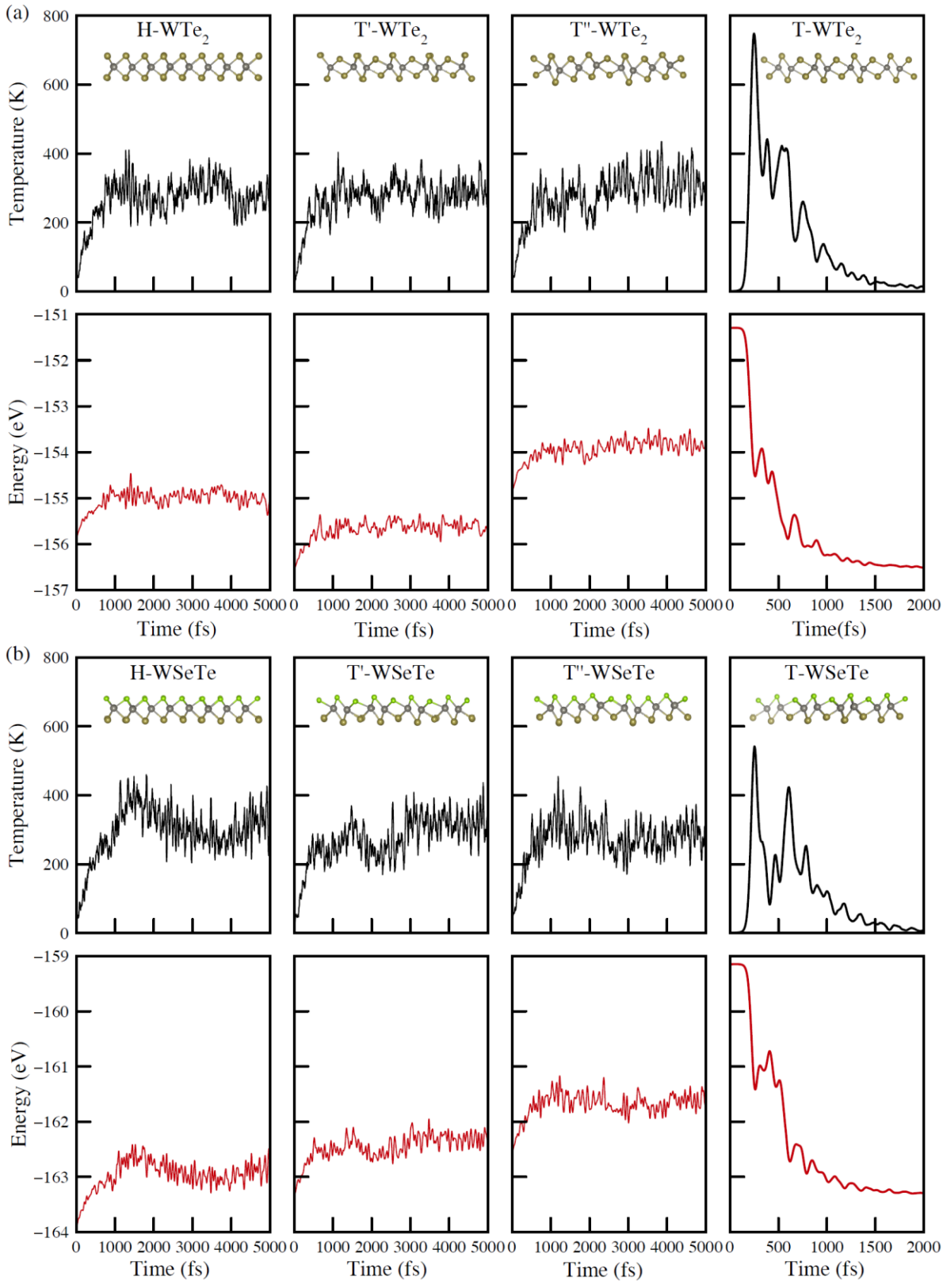

Figure 5. Temperature and total energy curves of AIMD simulations for all phases of (a) WTe_2 and (b) WSeTe. 300K simulations are shown here for H, T′ and T′′ phases, while 5K simulations for T phase as it spontaneously transforms into T′ phase.

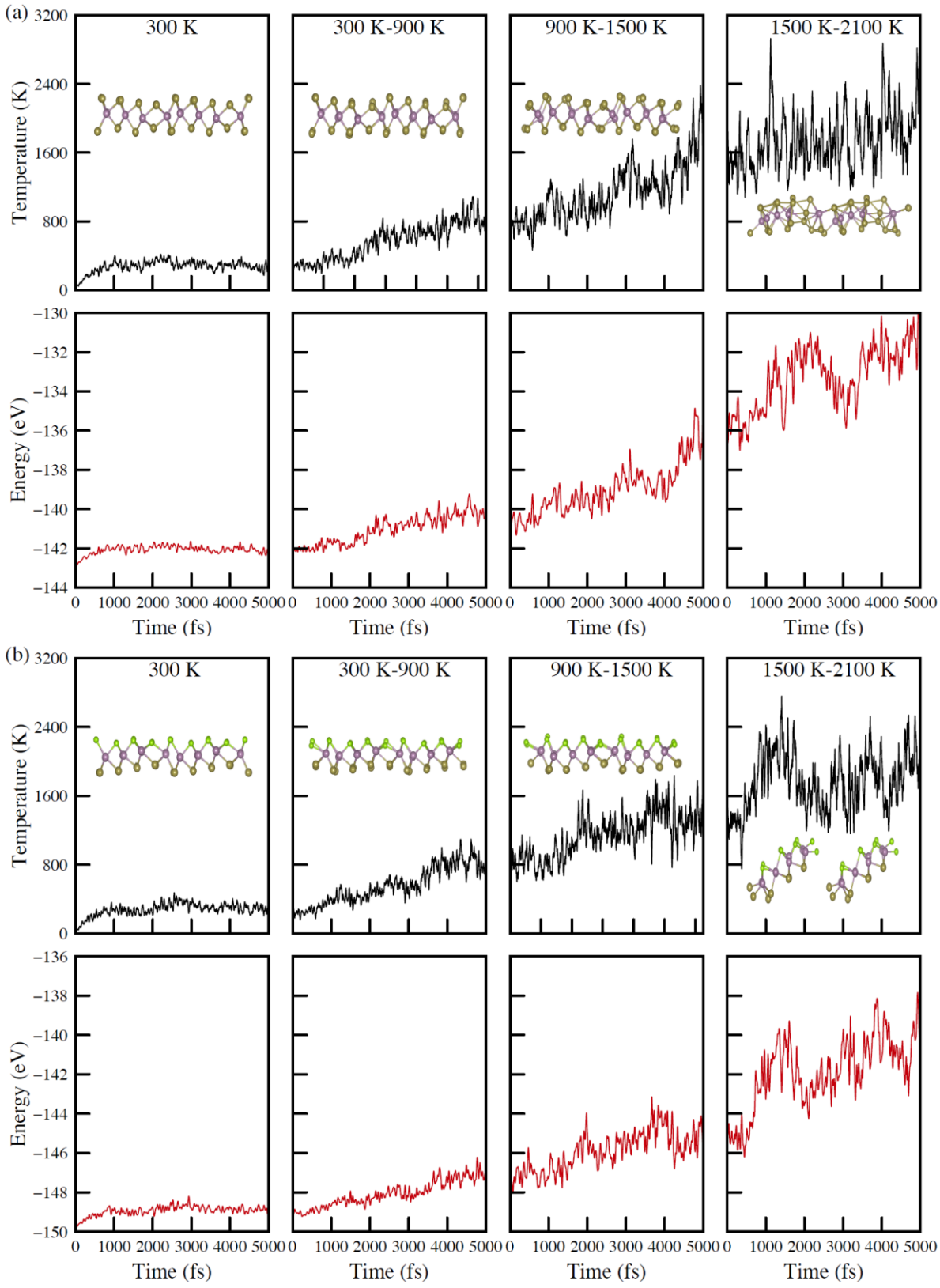

Figure 6. Temperature and total energy curves of AIMD simulations of heating up to 2100K for T'' phases of (a) $MoTe_2$ and (b) MoSeTe.

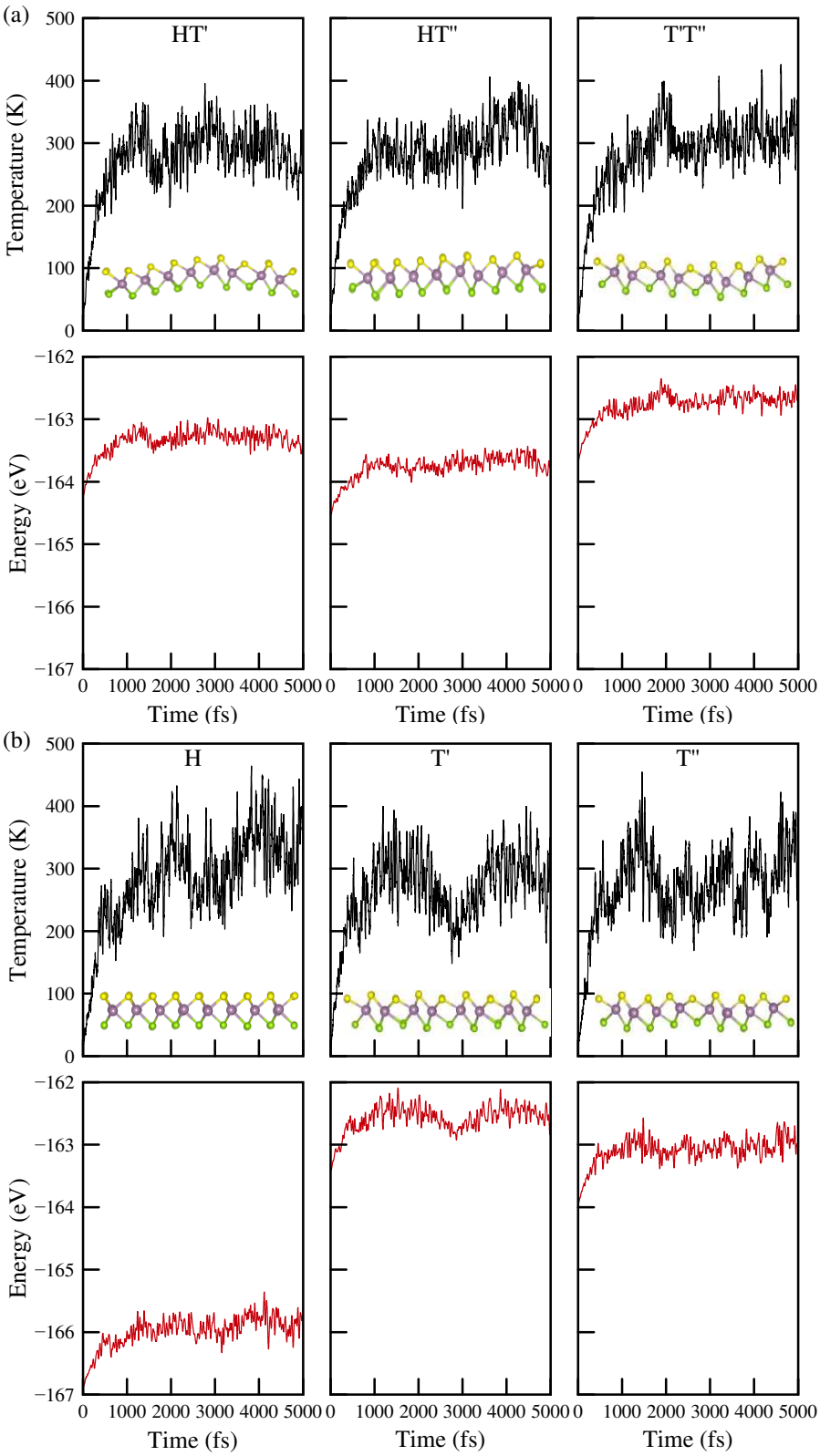

Figure 7. Temperature and total energy curves of AIMD simulations for (a) merged and (b) original H, T′ and T′′ phases of MoSSe Janus TMD. 300K simulations are shown for all phases and the total energy values of merged phases are divided by two to allow easier comparison to original phases.

Acknowledgements

Computational resources were provided by the High Performance and Grid Computing Center (TRGrid e-Infrastructure) of TUBITAK ULAKBIM and the National Center for High Performance Computing (UHeM) of Istanbul Technical University. ID and CS acknowledge the support from the Eskisehir Technical University (ESTU-BAP 20ADP210 and 20ADP246). ÖD would like to thank to the Council of Higher Education of Turkey (YÖK 100/2000) for doctoral scholarship.

Supporting Information

Ab-initio Molecular Dynamics (AIMD) simulation results as temperature, total energy, pressure and in-plane area variations for all considered TMD structures.

Author Contributions

The manuscript was written through contributions of all authors. All authors have given approval to the final version of the manuscript.

Conflicts of Interest

None.

References

(1) Novoselov, K. S.; Geim, A. K.; Morozov, S. V; Jiang, D.; Zhang, Y.; Dubonos, S. V; Grigorieva, I. V; Firsov, A. A. Electric Field Effect in Atomically Thin Carbon Films. *Science* **2004**, *306* (5696), 666–669. https://doi.org/10.1126/science.1102896.

(2) Geim, A. K.; Grigorieva, I. V. Van Der Waals Heterostructures. *Nature*. Nature Publishing Group July 24, 2013, pp 419–425. https://doi.org/10.1038/nature12385.

(3) Ramasubramaniam, A.; Naveh, D.; Towe, E. Tunable Band Gaps in Bilayer Transition-Metal Dichalcogenides. *Phys. Rev. B - Condens. Matter Mater. Phys.* **2011**, *84* (20). https://doi.org/10.1103/PhysRevB.84.205325.

(4) Radisavljevic, B.; Radenovic, A.; Brivio, J.; Giacometti, V.; Kis, A. Single-Layer MoS2 Transistors. *Nat. Nanotechnol.* **2011**, *6* (3), 147–150. https://doi.org/10.1038/nnano.2010.279.

(5) Tan, S. J. R.; Abdelwahab, I.; Ding, Z.; Zhao, X.; Yang, T.; Loke, G. Z. J.; Lin, H.; Verzhbitskiy, I.; Poh, S. M.; Xu, H.; Nai, C. T.; Zhou, W.; Eda, G.; Jia, B.; Loh, K. P. Chemical Stabilization of 1T′ Phase Transition Metal Dichalcogenides with Giant Optical Kerr Nonlinearity. *J. Am. Chem. Soc.* **2017**, *139* (6), 2504–2511. https://doi.org/10.1021/jacs.6b13238.

(6) Guan, Z.; Ni, S.; Hu, S. Tunable Electronic and Optical Properties of Monolayer and Multilayer Janus MoSSe as a Photocatalyst for Solar Water Splitting: A First-Principles Study. *J. Phys. Chem. C* **2018**, *122* (11), 6209–6216. https://doi.org/10.1021/acs.jpcc.8b00257.

(7) Shi, W.; Ye, J.; Zhang, Y.; Suzuki, R.; Yoshida, M.; Miyazaki, J.; Inoue, N.; Saito, Y.; Iwasa, Y. Superconductivity Series in Transition Metal Dichalcogenides by Ionic Gating. *Sci. Rep.* **2015**, *5*, 1–10. https://doi.org/10.1038/srep12534.
(8) Peng, X.; Peng, L.; Wu, C.; Xie, Y. Two Dimensional Nanomaterials for Flexible Supercapacitors. *Chem. Soc. Rev.* **2014**, *43* (10), 3303–3323. https://doi.org/10.1039/c3cs60407a.
(9) Liu, Y.; Gao, Y.; Zhang, S.; He, J.; Yu, J.; Liu, Z. Valleytronics in Transition Metal Dichalcogenides Materials. *Nano Research*. 2019, pp 2695–2711. https://doi.org/10.1007/s12274-019-2497-2.
(10) Bernardi, M.; Ataca, C.; Palummo, M.; Grossman, J. C. Optical and Electronic Properties of Two-Dimensional Layered Materials. *Nanophotonics* **2017**, *6* (2), 479–493. https://doi.org/10.1515/nanoph-2015-0030.
(11) Venkata Subbaiah, Y. P.; Saji, K. J.; Tiwari, A. Atomically Thin MoS 2 : A Versatile Nongraphene 2D Material . *Adv. Funct. Mater.* **2016**, *26* (13), 2046–2069. https://doi.org/10.1002/adfm.201504202.
(12) Yang, H.; Kim, S. W.; Chhowalla, M.; Lee, Y. H. Structural and Quantum-State Phase Transition in van Der Waals Layered Materials. *Nat. Phys.* **2017**, *13* (10), 931–937. https://doi.org/10.1038/nphys4188.
(13) Wang, R.; Yu, Y.; Zhou, S.; Li, H.; Wong, H.; Luo, Z.; Gan, L.; Zhai, T. Strategies on Phase Control in Transition Metal Dichalcogenides. *Adv. Funct. Mater.* **2018**, *28* (47). https://doi.org/10.1002/adfm.201802473.
(14) Li, Y.; Duerloo, K. A. N.; Wauson, K.; Reed, E. J. Structural Semiconductor-to-Semimetal Phase Transition in Two-Dimensional Materials Induced by Electrostatic Gating. *Nat. Commun.* **2016**, *7*, 1–8. https://doi.org/10.1038/ncomms10671.
(15) Mak, K. F.; Shan, J. Photonics and Optoelectronics of 2D Semiconductor Transition Metal Dichalcogenides. *Nat. Photonics* **2016**, *10* (4), 216–226. https://doi.org/10.1038/nphoton.2015.282.
(16) Lu, A. Y.; Zhu, H.; Xiao, J.; Chuu, C. P.; Han, Y.; Chiu, M. H.; Cheng, C. C.; Yang, C. W.; Wei, K. H.; Yang, Y.; Wang, Y.; Sokaras, D.; Nordlund, D.; Yang, P.; Muller, D. A.; Chou, M. Y.; Zhang, X.; Li, L. J. Janus Monolayers of Transition Metal Dichalcogenides. *Nat. Nanotechnol.* **2017**, *12* (8), 744–749. https://doi.org/10.1038/nnano.2017.100.
(17) Suzuki, R.; Sakano, M.; Zhang, Y. J.; Akashi, R.; Morikawa, D.; Harasawa, A.; Yaji, K.; Kuroda, K.; Miyamoto, K.; Okuda, T.; Ishizaka, K.; Arita, R.; Iwasa, Y. Valley-Dependent Spin Polarization in Bulk MoS 2 with Broken Inversion Symmetry. *Nat. Nanotechnol.* **2014**, *9* (8), 611–617. https://doi.org/10.1038/nnano.2014.148.
(18) Dong, L.; Lou, J.; Shenoy, V. B. Large In-Plane and Vertical Piezoelectricity in Janus Transition Metal Dichalchogenides. *ACS Nano* **2017**, *11* (8), 8242–8248. https://doi.org/10.1021/acsnano.7b03313.
(19) Xia, C.; Xiong, W.; Du, J.; Wang, T.; Peng, Y.; Li, J. Universality of Electronic Characteristics and Photocatalyst Applications in the Two-Dimensional Janus Transition Metal Dichalcogenides. *Phys. Rev. B* **2018**, *98* (16). https://doi.org/10.1103/PhysRevB.98.165424.
(20) Zhang, J.; Jia, S.; Kholmanov, I.; Dong, L.; Er, D.; Chen, W.; Guo, H.; Jin, Z.; Shenoy, V. B.; Shi, L.; Lou, J. Janus Monolayer Transition-Metal Dichalcogenides. *ACS Nano* **2017**, *11* (8), 8192–8198. https://doi.org/10.1021/acsnano.7b03186.
(21) Trivedi, D. B.; Turgut, G.; Qin, Y.; Sayyad, M. Y.; Hajra, D.; Howell, M.; Liu, L.; Yang, S.; Patoary, N. H.; Li, H.; Petrić, M. M.; Meyer, M.; Kremser, M.; Barbone, M.; Soavi, G.; Stier, A. V.; Müller, K.; Yang, S.; Esqueda, I. S.; Zhuang, H.; Finley, J. J.; Tongay, S. Room-Temperature Synthesis of 2D Janus Crystals and Their

Heterostructures. *Adv. Mater.* **2020**, *32* (50), 2006320. https://doi.org/10.1002/adma.202006320.
(22) Li, R.; Cheng, Y.; Huang, W. Recent Progress of Janus 2D Transition Metal Chalcogenides: From Theory to Experiments. *Small*. Wiley-VCH Verlag November 8, 2018, p 1802091. https://doi.org/10.1002/smll.201802091.
(23) Zhang, K.; Bao, C.; Gu, Q.; Ren, X.; Zhang, H.; Deng, K.; Wu, Y.; Li, Y.; Feng, J.; Zhou, S. Raman Signatures of Inversion Symmetry Breaking and Structural Phase Transition in Type-II Weyl Semimetal MoTe 2. *Nat. Commun.* **2016**, *7*, 1–6. https://doi.org/10.1038/ncomms13552.
(24) Leng, K.; Chen, Z.; Zhao, X.; Tang, W.; Tian, B.; Nai, C. T.; Zhou, W.; Loh, K. P. Phase Restructuring in Transition Metal Dichalcogenides for Highly Stable Energy Storage. *ACS Nano* **2016**, *10* (10), 9208–9215. https://doi.org/10.1021/acsnano.6b05746.
(25) Eda, G.; Fujita, T.; Yamaguchi, H.; Voiry, D.; Chen, M.; Chhowalla, M. Coherent Atomic and Electronic Heterostructures of Single-Layer MoS 2. *ACS Nano* **2012**, *6* (8), 7311–7317. https://doi.org/10.1021/nn302422x.
(26) Kappera, R.; Voiry, D.; Yalcin, S. E.; Branch, B.; Gupta, G.; Mohite, A. D.; Chhowalla, M. Phase-Engineered Low-Resistance Contacts for Ultrathin MoS2 Transistors. *Nat. Mater.* **2014**, *13* (12), 1128–1134. https://doi.org/10.1038/nmat4080.
(27) Kresse, G.; Hafner, J. Ab Initio Molecular Dynamics for Liquid Metals. *Phys. Rev. B* **1993**, *47* (1), 558–561. https://doi.org/10.1103/PhysRevB.47.558.
(28) Kresse, G.; Hafner, J. Ab Initio Molecular-Dynamics Simulation of the Liquid-Metalamorphous- Semiconductor Transition in Germanium. *Phys. Rev. B* **1994**, *49* (20), 14251–14269. https://doi.org/10.1103/PhysRevB.49.14251.
(29) Kresse, G.; Furthmüller, J. Efficient Iterative Schemes for Ab Initio Total-Energy Calculations Using a Plane-Wave Basis Set. *Phys. Rev. B - Condens. Matter Mater. Phys.* **1996**, *54* (16), 11169–11186. https://doi.org/10.1103/PhysRevB.54.11169.
(30) Perdew, J. P.; Burke, K.; Ernzerhof, M. Generalized Gradient Approximation Made Simple. *Phys. Rev. Lett.* **1996**, *77* (18), 3865–3868. https://doi.org/10.1103/PhysRevLett.77.3865.
(31) Pack, J. D.; Monkhorst, H. J. "special Points for Brillouin-Zone Integrations"-a Reply. *Phys. Rev. B* **1977**, *16* (4), 1748–1749. https://doi.org/10.1103/PhysRevB.16.1748.
(32) Kresse, G.; Joubert, D. From Ultrasoft Pseudopotentials to the Projector Augmented-Wave Method. *Phys. Rev. B* **1999**, *59* (3), 1758–1775. https://doi.org/10.1103/PhysRevB.59.1758.
(33) Blöchl, P. E. Projector Augmented-Wave Method. *Phys. Rev. B* **1994**, *50* (24), 17953–17979. https://doi.org/10.1103/PhysRevB.50.17953.
(34) Henkelman, G.; Jónsson, H. A Dimer Method for Finding Saddle Points on High Dimensional Potential Surfaces Using Only First Derivatives. *J. Chem. Phys.* **1999**, *111* (15), 7010–7022. https://doi.org/10.1063/1.480097.
(35) Henkelman, G.; Uberuaga, B. P.; Jónsson, H. Climbing Image Nudged Elastic Band Method for Finding Saddle Points and Minimum Energy Paths. *J. Chem. Phys.* **2000**, *113* (22), 9901–9904. https://doi.org/10.1063/1.1329672.
(36) Heyes, D. M. Molecular Dynamics at Constant Pressure and Temperature. *Chem. Phys.* **1983**, *82* (3), 285–301. https://doi.org/10.1016/0301-0104(83)85235-5.
(37) Huang, H. H.; Fan, X.; Singh, D. J.; Chen, H.; Jiang, Q.; Zheng, W. T. Controlling Phase Transition for Single-Layer MTe2 (M = Mo and W): Modulation of the Potential Barrier under Strain. *Phys. Chem. Chem. Phys.* **2016**, *18* (5), 4086–4094. https://doi.org/10.1039/c5cp06706e.
(38) Patil, U.; Caffrey, N. M. Composition Dependence of the Charge-Driven Phase

Transition in Group-VI Transition Metal Dichalcogenides. *Phys. Rev. B* **2019**, *100* (7). https://doi.org/10.1103/PhysRevB.100.075424.
(39) Qian, X.; Liu, J.; Fu, L.; Li, J. Quantum Spin Hall Effect in Two - Dimensional Transition Metal Dichalcogenides. *Science (80-.).* **2014**, *346* (6215), 1344–1347. https://doi.org/10.1126/science.1256815.
(40) García, Á. M.; Corro, E. Del; Kalbac, M.; Frank, O. Tuning the Electronic Properties of Monolayer and Bilayer Transition Metal Dichalcogenide Compounds under Direct Out-of-Plane Compression. *Phys. Chem. Chem. Phys.* **2017**, *19* (20), 13333–13340. https://doi.org/10.1039/c7cp00012j.
(41) Ji, Y.; Yang, M.; Lin, H.; Hou, T.; Wang, L.; Li, Y.; Lee, S. T. Janus Structures of Transition Metal Dichalcogenides as the Heterojunction Photocatalysts for Water Splitting. *J. Phys. Chem. C* **2018**, *122* (5), 3123–3129. https://doi.org/10.1021/acs.jpcc.7b11584.
(42) Wang, D.; Liu, L.; Basu, N.; Zhuang, H. L. High-Throughput Computational Characterization of 2D Compositionally Complex Transition-Metal Chalcogenide Alloys. *Adv. Theory Simulations* **2020**, *3* (11), 2000195. https://doi.org/10.1002/adts.202000195.
(43) Tang, X.; Li, S.; Ma, Y.; Du, A.; Liao, T.; Gu, Y.; Kou, L. Distorted Janus Transition Metal Dichalcogenides: Stable Two-Dimensional Materials with Sizable Band Gap and Ultrahigh Carrier Mobility. *J. Phys. Chem. C* **2018**, *122* (33), 19153–19160. https://doi.org/10.1021/acs.jpcc.8b04161.
(44) Kan, M.; Nam, H. G.; Lee, Y. H.; Sun, Q. Phase Stability and Raman Vibration of the Molybdenum Ditelluride (MoTe2) Monolayer. *Phys. Chem. Chem. Phys.* **2015**, *17* (22), 14866–14871. https://doi.org/10.1039/c5cp01649e.
(45) Zulfiqar, M.; Zhao, Y.; Li, G.; Li, Z. C.; Ni, J. Intrinsic Thermal Conductivities of Monolayer Transition Metal Dichalcogenides MX 2 (M = Mo, W; X = S, Se, Te). *Sci. Rep.* **2019**, *9* (1), 1–7. https://doi.org/10.1038/s41598-019-40882-2.
(46) Ouyang, B.; Chen, S.; Jing, Y.; Wei, T.; Xiong, S.; Donadio, D. Enhanced Thermoelectric Performance of Two Dimensional MS2 (M = Mo, W) through Phase Engineering. *J. Mater.* **2018**, *4* (4), 329–337. https://doi.org/10.1016/j.jmat.2018.08.001.
(47) Xiang, H.; Xu, B.; Liu, J.; Xia, Y.; Lu, H.; Yin, J.; Liu, Z. Quantum Spin Hall Insulator Phase in Monolayer WTe2 by Uniaxial Strain. *AIP Adv.* **2016**, *6* (9), 095005. https://doi.org/10.1063/1.4962662.
(48) Wang, Z. 2H → 1T′ Phase Transformation in Janus Monolayer MoSSe and MoSTe: An Efficient Hole Injection Contact for 2H-MoS2. *J. Mater. Chem. C* **2018**, *6* (47), 13000–13005. https://doi.org/10.1039/C8TC04951C.
(49) Ma, F.; Gao, G.; Jiao, Y.; Gu, Y.; Bilic, A.; Zhang, H.; Chen, Z.; Du, A. Predicting a New Phase (T″) of Two-Dimensional Transition Metal Di-Chalcogenides and Strain-Controlled Topological Phase Transition. *Nanoscale* **2016**, *8* (9), 4969–4975. https://doi.org/10.1039/C5NR07715J.
(50) Pandey, M.; Bothra, P.; Pati, S. K. Phase Transition of MoS2 Bilayer Structures. *J. Phys. Chem. C* **2016**, *120* (7), 3776–3780. https://doi.org/10.1021/acs.jpcc.5b10904.
(51) Krishnamoorthy, A.; Bassman, L.; Kalia, R. K.; Nakano, A.; Shimojo, F.; Vashishta, P. Semiconductor-Metal Structural Phase Transformation in MoTe2 Monolayers by Electronic Excitation. *Nanoscale* **2018**, *10* (6), 2742–2747. https://doi.org/10.1039/c7nr07890k.
(52) Duerloo, K. A. N.; Reed, E. J. Structural Phase Transitions by Design in Monolayer Alloys. *ACS Nano* **2016**, *10* (1), 289–297. https://doi.org/10.1021/acsnano.5b04359.
(53) Aierken, Y.; Sevik, C.; Gülseren, O.; Peeters, F. M.; Çakir, D. In Pursuit of Barrierless

Transition Metal Dichalcogenides Lateral Heterojunctions. *Nanotechnology* **2018**, *29* (29), 295202. https://doi.org/10.1088/1361-6528/aac17d.